Second-order Semi-implicit Projection Methods for Landau-Lifshitz Equation

Changjian Xie

School of Mathematical Sciences, Soochow University

Joint work with

Jingrun Chen (Soochow University)
Carlos García-Cervera (UC, Santa Barbara)
Cheng Wang (University of Massachusetts)
Zhennan Zhou (Peking University)

September 21, 2019, CSIAM 2019, Foshan

Outline

Outline

Magnetic recording devices and computer storages

- Spinvalues[1]

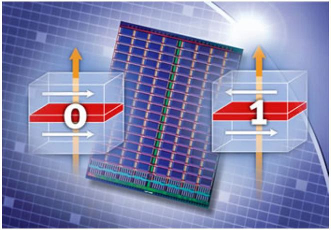

Magnetoresistance random access memory (MRAM)

- Domain walls [2]

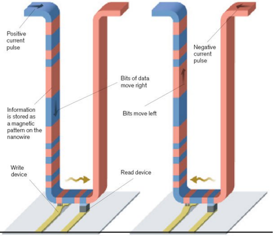

Racetrack memories

[1] Science@Berkeley Lab: The Current Spin on Spintronics

[2] http://www2.technologyreview.com/article/412189/tr10-racetrack-memory/

Methodology for detecting the orientation

- Tunnel magnetoresistance [3]

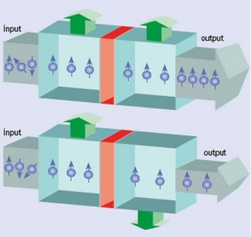

Julliere's model: Constant tunneling matrix

$$TMR \equiv \frac{G_{AP} - G_P}{G_{AP}} = \frac{2P_L P_R}{1 - P_L P_R}$$

$$P_L = \frac{n_L^{\uparrow} - n_L^{\downarrow}}{n_L^{\uparrow} + n_L^{\downarrow}} \qquad P_R = \frac{n_R^{\uparrow} - n_R^{\downarrow}}{n_R^{\uparrow} + n_R^{\downarrow}}$$

- Gaint magnetoresistance [4]

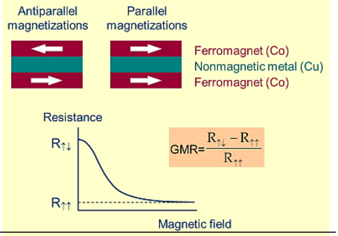

- Albert Fert and Peter Grüberg: 2007 Nobel Prize in Physics
- Polarization and scattering

[3] http://ducthe.wordpress.com/category/spintronics/

[4] http://physics.unl.edu/

Methodology for rotating the orientation

- Spin transfer torque (STT) [5]

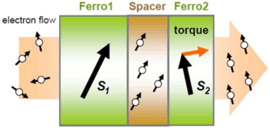

  - Two layers of different thickness: different switching fields
  - The thin film is switched, and the resistance measured

- Current-driven domain wall motion [6]

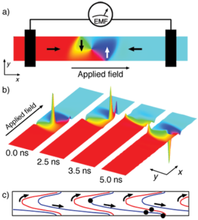

  - Applied current supplies spin transfer torques

[5] http://www.wpi-aimr.tohoku.ac.jp/miyazaki_ labo/spintorque.htm

[6] http://physics.aps.org/articles/v2/11

Basic quantity of interest:

$$\boldsymbol{m} : \Omega \longrightarrow \mathbb{R}^3; \quad |\boldsymbol{m}| = 1$$

Landau-Lifshitz energy functional:

$$\begin{aligned} F_{\mathrm{LL}}[\boldsymbol{m}] &= \frac{K_u}{M_s}\int_\Omega \phi(\boldsymbol{m})\, dx + \frac{C_{\mathrm{ex}}}{M_s}\int_\Omega |\nabla \boldsymbol{m}|^2\, dx \\ &- \frac{\mu_0}{2} M_s \int_\Omega \boldsymbol{h}_s \cdot \boldsymbol{m}\, dx - \mu_0 M_s \int_\Omega \boldsymbol{h}_e \cdot \boldsymbol{m}\, dx \end{aligned}$$

- Continuum theory.
- Domain structure $\longleftrightarrow$ Local minimizers.

- $\phi(\boldsymbol{m})$: Anisotropy Energy: Penalizes deviations from the easy directions. For uniaxial materials $\phi(\boldsymbol{m}) = \left(m_2^2 + m_3^2\right)$.
- $\frac{C_{\text{ex}}}{M_s}|\nabla \boldsymbol{m}|^2$: Exchange energy: Penalizes spatial variations.
- $-\mu_0 M_s \boldsymbol{h}_e \cdot \boldsymbol{m}$: External field (Zeeman) energy.
- $-\frac{\mu_0}{2} M_s \boldsymbol{h}_s \cdot \boldsymbol{m}$: Stray field (self-induced) energy.
- The stray field, $\boldsymbol{h}_s = -\nabla u$ is obtained by solving the magnetostatic equation:

$$\Delta u = \text{div } \boldsymbol{m}, \quad \boldsymbol{x} \in \Omega, \quad \Delta u = 0, \quad \boldsymbol{x} \in \overline{\Omega}^c$$

with jump boundary conditions

$$[u]_{\partial\Omega} = 0, \quad \left[\frac{\partial u}{\partial \nu}\right]_{\partial\Omega} = -\boldsymbol{m} \cdot \nu.$$

Landau-Lifshitz equation

- Torque balance

$$\boldsymbol{m}_t = -\boldsymbol{m} \times \boldsymbol{h} + \alpha \boldsymbol{m} \times \boldsymbol{m}_t,$$

or equivalently,

$$\boldsymbol{m}_t = -\frac{1}{1+\alpha^2}\boldsymbol{m} \times \boldsymbol{h} - \frac{\alpha}{1+\alpha^2}\boldsymbol{m} \times (\boldsymbol{m} \times \boldsymbol{h}),$$

where

$$\boldsymbol{h} = -\frac{\delta F_{\mathrm{LL}}}{\delta \boldsymbol{m}} = -Q(m_2\boldsymbol{e}_2 + m_2\boldsymbol{e}_3) + \epsilon \Delta \boldsymbol{m} + \boldsymbol{h}_{\mathrm{s}} + \boldsymbol{h}_{\mathrm{e}}$$

and the second term is the Gilbert damping term.

- $\alpha << 1$: Damping coefficient

Model problem

$$\boldsymbol{m}_t = -\boldsymbol{m} \times \Delta \boldsymbol{m} + \alpha \boldsymbol{m} \times \boldsymbol{m}_t,$$

or

$$\boldsymbol{m}_t = -\boldsymbol{m} \times \Delta \boldsymbol{m} - \alpha \boldsymbol{m} \times (\boldsymbol{m} \times \Delta \boldsymbol{m})$$

with the Neumann boundary condition and the constraint $|\boldsymbol{m}| = 1$.

Literature review: Mathematical aspect

1. Existence of weak solutions: [Alouges and Soyeur, 1992] in 3D whole space and [Guo and Hong, 1993] in 2D bounded domain;
2. Nonuniqueness of weak solutions: [Alouges and Soyeur, 1992];
3. Local existence and uniqueness; global existence and uniqueness with small-energy initial data of strong solutions: [Carbou and Fabrie, 2001a] in 3D whole space; [Carbou and Fabrie, 2001b] in 2D bounded domain.

Literature review: Numerical aspect

Review articles: [Kruzík and Prohl, 2006; Cimrák, 2008]

- Finite element: [Bartels and Prohl, 2006; Alouges, 2008; Cimrák, 2009];
- Finite difference: [E and Wang, 2001; Fuwa et al., 2012; Kim and Lipnikov, 2017];

Linearity of the discrete system:

- Explicit scheme: [Jiang et al., 2001; Alouges and Jaisson, 2006];
- Fully implicit scheme: [Prohl, 2001; Bartels and Prohl, 2006; Fuwa et al., 2012];
- Semi-implicit scheme: [Wang, Garcia-Cervera, and E, 2001; E and Wang, 2001; Gao, 2014; Lewis and Nigam, 2003; Cimrák, 2005].

Continued...

Time marching

- Splitting method: [Wang, Garcia-Cervera, and E, 2001];
- Mid-point method: [Bertotti et al., 2001, d'Aquino et al., 2005];
- Runge-Kutta methods: [Romeo et al., 2008];
- Geometric integration methods: [Jiang, Kaper, and Leaf, 2001];

Convergence analysis

- 1st order in time + 2nd order in space: [Alouges, 2008];
- 2nd order in time + 2nd order in space: [Bertotti et al., 2001, d'Aquino et al., 2005, Bartels and Prohl, 2006, Fuwa et al., 2012];
  - Unconditional stability;
  - Nonlinear solver at each time step (unavailable theoretical justification of the unique solvability);
  - Step-size condition $k = \mathcal{O}(h^2)$ with k the temporal stepsize and h the spatial stepsize;

Outline

Spatial discretization

- $x_i = ih$, $i = 0, 1, 2, \cdots, N_x$, with $x_0 = 0$, $x_{N_x} = 1$;
- $\hat{x}_i = x_{i-1/2} = (i - 1/2)h$, $i = 1, \cdots, N_x$;
- $\boldsymbol{m}_i^n \approx \boldsymbol{m}(\hat{x}_i, t^n)$;
- $\Delta_h \boldsymbol{m}_i = \frac{\boldsymbol{m}_{i+1} - 2\boldsymbol{m}_i + \boldsymbol{m}_{i-1}}{h^2}$;
- Third order extrapolation for boundary condition:

$$\boldsymbol{m}_1 = \boldsymbol{m}_0, \quad \boldsymbol{m}_{N_x+1} = \boldsymbol{m}_{N_x}.$$

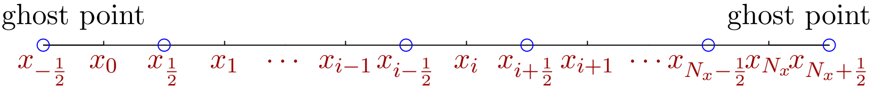

Figure 1: Illustration of the 1-D spatial mesh.

Semi-implicit projection methods [Xie, García-Cervera, Wang, Zhou, and Chen, submitted, 2019]

- $\boldsymbol{m}_t = -\boldsymbol{m} \times \Delta \boldsymbol{m} + \alpha \boldsymbol{m} \times \boldsymbol{m}_t$:

$$\left(1 - \alpha \hat{\boldsymbol{m}}_h^{n+2} \times\right) \frac{\frac{3}{2}\boldsymbol{m}_h^{n+2,*} - 2\boldsymbol{m}_h^{n+1} + \frac{1}{2}\boldsymbol{m}_h^n}{k} = -\hat{\boldsymbol{m}}_h^{n+2} \times \Delta_h \boldsymbol{m}_h^{n+2,*},$$
$$\hat{\boldsymbol{m}}_h^{n+2} = 2\boldsymbol{m}_h^{n+1} - \boldsymbol{m}_h^n;$$

- $\boldsymbol{m}_t = -\boldsymbol{m} \times \Delta \boldsymbol{m} - \alpha \boldsymbol{m} \times (\boldsymbol{m} \times \Delta \boldsymbol{m})$:

$$\frac{\frac{3}{2}\boldsymbol{m}_h^{n+2,*} - 2\boldsymbol{m}_h^{n+1} + \frac{1}{2}\boldsymbol{m}_h^n}{k} = -\hat{\boldsymbol{m}}_h^{n+2} \times \Delta_h \boldsymbol{m}_h^{n+2,*} - \alpha \hat{\boldsymbol{m}}_h^{n+2} \times \left(\hat{\boldsymbol{m}}_h^{n+2} \times \Delta_h \boldsymbol{m}_h^{n+2,*}\right);$$

- A projection step: $\boldsymbol{m}_h^{n+2} = \frac{\boldsymbol{m}_h^{n+2,*}}{|\boldsymbol{m}_h^{n+2,*}|}$.

1D test: Accuracy

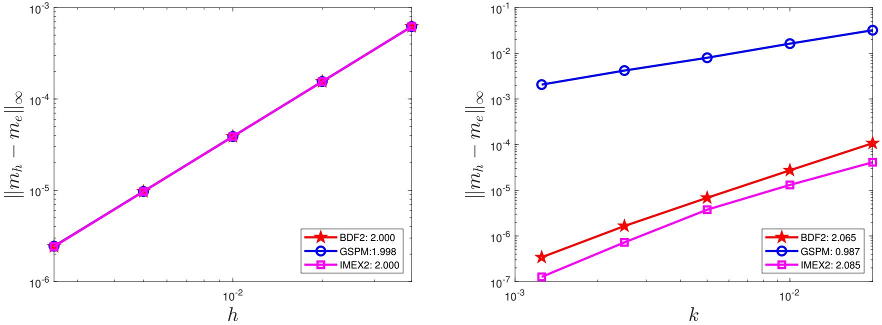

Figure 2: Accuracy of BDF2, GSPM and IMEX2. They are all second-order accurate in space. GSPM is first-order accurate in time. BDF2 and IMEX2 are second-order accurate in time.

1D test: Efficiency

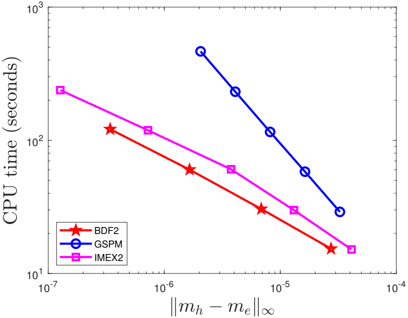

Figure 3: CPU time (in seconds) of BDF2, GSPM and IMEX2 versus error $\|\boldsymbol{m}_h - \boldsymbol{m}_e\|_\infty$. For a given tolerance of error, costs of these schemes in the increasing order are: BDF2 $<$ IMEX2 $<$ GSPM.

3D test: Accuracy

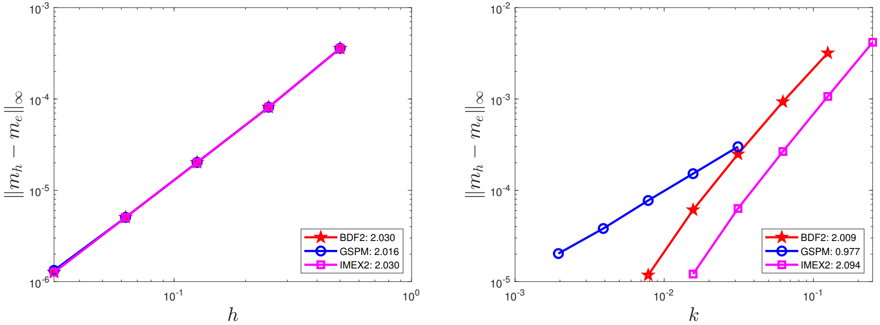

Figure 4: Accuracy of BDF2, GSPM and IMEX2. They are all second-order accurate in space. GSPM is first-order accurate in time. BDF2 and IMEX2 are second-order accurate in time.

3D test: Efficiency

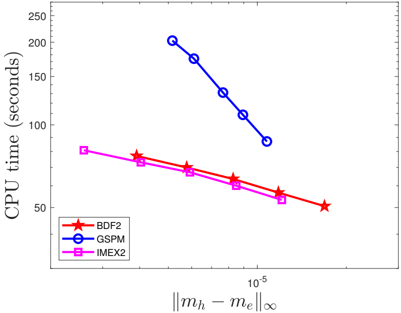

Figure 5: CPU time (in seconds) of BDF2, GSPM and IMEX2 versus error $\|\boldsymbol{m}_h - \boldsymbol{m}_e\|_\infty$. For a given tolerance of error, costs of BDF2$\approx$ IMEX2$<$GSPM when $h_x = h_y = h_z = 1/16$ in 3D.

Outline

Mumag standard problem 1

Ask for simulating hysteresis loops.[7]

- Geometry: $1 \times 2 \times 0.02$ micron rectangle
- Material parameters: To mimic permalloy

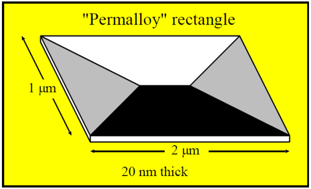

Exchange constant: $C_{ex} = 1.3 \times 10^{-11}$ J/m

Saturation magnetization: $M_s = 8.0 \times 10^5$ A/m

Anisotropy constant: $K_u = 5.0 \times 10^2$ J/m^3

Permeability of vacuum: $\mu_0 = 4\pi \times 10^{-7}$ N/A^2

Damping parameter: $\alpha = 0.1$

Uniaxial, with easy axis nominally parallel to the long edges of the rectangle.

[7] https://www.ctcms.nist.gov/∼rdm/mumag.org.html

Setup for our simulations

- The film of size: $1\ \mu\text{m} \times 2\ \mu\text{m} \times 200\ \text{Å}$;
- The cell of size: $20\ \text{nm} \times 20\ \text{nm} \times 20\ \text{nm}$;
- Timescale: $k = 1$ ps;
- \# of field states: 133 for $x-$ loop (or $y-$ loop).
- For hysteresis loops simulation: the applied field H_0 (begin from 500 Oe) approximately parallel (canting angle $+1^\circ$) along $y-$ (long) axis and $x-$ (short) axis.

Semi-implicit projection methods for full LL equation

- $\boldsymbol{m}_t = -\boldsymbol{m} \times \boldsymbol{h} + \alpha \boldsymbol{m} \times \boldsymbol{m}_t$:

$$\left(1 - \alpha \hat{\boldsymbol{m}}_h^{n+2} \times\right) \frac{\frac{3}{2}\boldsymbol{m}_h^{n+2,*} - 2\boldsymbol{m}_h^{n+1} + \frac{1}{2}\boldsymbol{m}_h^n}{k} = -\hat{\boldsymbol{m}}_h^{n+2} \times \left(\epsilon \Delta_h \boldsymbol{m}_h^{n+2,*} + \hat{\boldsymbol{f}}_h^{n+2}\right),$$

$$\hat{\boldsymbol{m}}_h^{n+2} = 2\boldsymbol{m}_h^{n+1} - \boldsymbol{m}_h^n,$$

$$\hat{\boldsymbol{f}}_h^{n+2} = 2\boldsymbol{f}_h^{n+1} - \boldsymbol{f}_h^n,$$

$$\boldsymbol{f}_h^n = -Q(m_2^n \boldsymbol{e}_2 + m_3^n \boldsymbol{e}_3) + \boldsymbol{h}_s^n + \boldsymbol{h}_e^n;$$

- $\boldsymbol{m}_t = -\boldsymbol{m} \times \boldsymbol{h} - \alpha \boldsymbol{m} \times (\boldsymbol{m} \times \boldsymbol{h})$:

$$\frac{\frac{3}{2}\boldsymbol{m}_h^{n+2,*} - 2\boldsymbol{m}_h^{n+1} + \frac{1}{2}\boldsymbol{m}_h^n}{k} = -\hat{\boldsymbol{m}}_h^{n+2} \times \left(\epsilon \Delta_h \boldsymbol{m}_h^{n+2,*} + \hat{\boldsymbol{f}}_h^{n+2}\right)$$
$$- \alpha \hat{\boldsymbol{m}}_h^{n+2} \times \left(\hat{\boldsymbol{m}}_h^{n+2} \times \left(\epsilon \Delta_h \boldsymbol{m}_h^{n+2,*} + \hat{\boldsymbol{f}}_h^{n+2}\right)\right);$$

- A projection step: $\boldsymbol{m}_h^{n+2} = \dfrac{\boldsymbol{m}_h^{n+2,*}}{|\boldsymbol{m}_h^{n+2,*}|}$.

mo96a:

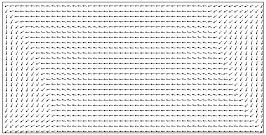

(a) $H_0//y\text{-}axis$

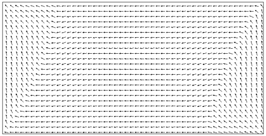

(b) $H_0//x\text{-}axis$

BDF2:

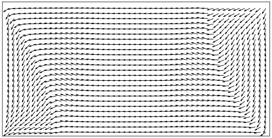

(c) $H_0//y\text{-}axis$

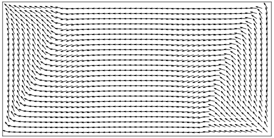

(d) $H_0//x\text{-}axis$

Figure 6: The in-plane magnetization components are represented by arrows.

Magnetization profile (cont'd)

mo96a:

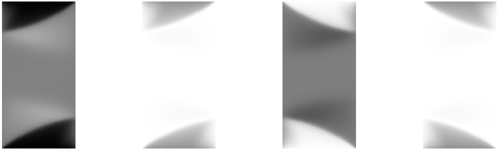

(a) m_x $(H_0//y\text{-}axis)$ (b) m_y $(H_0//y\text{-}axis)$ (c) m_x $(H_0//x\text{-}axis)$ (d) m_y $(H_0//x\text{-}axis)$

BDF2:

(e) m_x $(H_0//y\text{-}axis)$ (f) m_y $(H_0//y\text{-}axis)$ (g) m_x $(H_0//x\text{-}axis)$ (h) m_y $(H_0//x\text{-}axis)$

Figure 7: The x- and y- magnetization components are visualized by the gray value.

Hysteresis loop

mo96a:

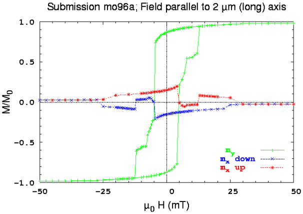

(a) $H_0//y\text{-}axis$

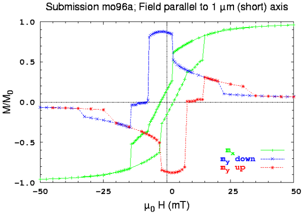

(b) $H_0//x\text{-}axis$

BDF2:

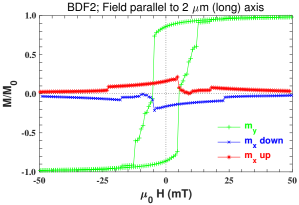

(c) $H_0//y\text{-}axis$

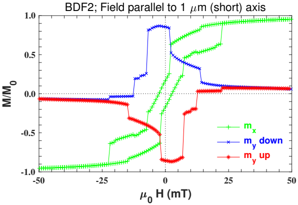

(d) $H_0//x\text{-}axis$

Semi-implicit projection methods revisited

- Lack of numerical stability of Lax-Richtmyer type;
- Separation of the time-marching step and the projection step:

$$\begin{aligned}
&\frac{\frac{3}{2}\tilde{\boldsymbol{m}}_h^{n+2} - 2\tilde{\boldsymbol{m}}_h^{n+1} + \frac{1}{2}\tilde{\boldsymbol{m}}_h^{n}}{k} = -\hat{\boldsymbol{m}}_h^{n+2} \times \Delta_h \tilde{\boldsymbol{m}}_h^{n+2} \\
&\quad - \alpha \hat{\boldsymbol{m}}_h^{n+2} \times (\hat{\boldsymbol{m}}_h^{n+2} \times \Delta_h \tilde{\boldsymbol{m}}_h^{n+2}), \\
&\quad \hat{\boldsymbol{m}}_h^{n+2} = 2\boldsymbol{m}_h^{n+1} - \boldsymbol{m}_h^{n}, \\
&\quad \boldsymbol{m}_h^{n+2} = \frac{\tilde{\boldsymbol{m}}_h^{n+2}}{|\tilde{\boldsymbol{m}}_h^{n+2}|};
\end{aligned}$$

- Two sets of approximations $\tilde{\boldsymbol{m}}_h^n$ and $\boldsymbol{m}_h^n$.

1D test

$$\boldsymbol{m}_e = \left(\cos(x^2(1-x)^2)\sin t, \sin(x^2(1-x)^2)\sin t, \cos t\right)^T$$

Table 1: Accuracy of our method on the uniform mesh when $h = k$ and $\alpha = 0.01$.

k	$\|\boldsymbol{m}_h - \boldsymbol{m}_e\|_\infty$	$\|\boldsymbol{m}_h - \boldsymbol{m}_e\|_2$	$\|\boldsymbol{m}_h - \boldsymbol{m}_e\|_{H^1}$
5.0D-3	3.867D-5	4.115D-5	1.729D-4
2.5D-3	7.976D-6	1.053D-5	4.629D-5
1.25D-3	2.135D-6	2.648D-6	1.177D-5
6.25D-4	5.765D-7	6.627D-7	2.949D-6
3.125D-4	1.447D-7	1.657D-7	7.370D-7
order	1.991	1.990	1.972

Outline

Definitions

- Inner product and $\|\cdot\|_2$ norm

$$\langle \boldsymbol{f}_h, \boldsymbol{g}_h \rangle = h^d \sum_{\mathcal{I} \in \Lambda_d} \boldsymbol{f}_{\mathcal{I}} \cdot \boldsymbol{g}_{\mathcal{I}},$$
$$\|\boldsymbol{f}_h\|_2 = (\langle \boldsymbol{f}_h, \boldsymbol{f}_h \rangle)^{1/2};$$

- Discrete $\|\cdot\|_\infty$ norm: $\|\boldsymbol{f}_h\|_\infty = \max_{\mathcal{I} \in \Lambda_d} \|\boldsymbol{f}_{\mathcal{I}}\|_\infty$;
- Average: $\overline{\boldsymbol{f}}_h = h^d \sum_{\mathcal{I} \in \Lambda_d} \boldsymbol{f}_{\mathcal{I}}$;
- Discrete H_h^{-1}-norm: $\|\boldsymbol{f}_h\|_{-1}^2 = \langle (-\Delta_h)^{-1} \boldsymbol{f}_h, \boldsymbol{f}_h \rangle$.

Preliminary estimates

- Inverse inequality:
  $\|\boldsymbol{e}_h^n\|_\infty \leq h^{-d/2}\|\boldsymbol{e}_h^n\|_2, \quad \|\nabla_h \boldsymbol{e}_h^n\|_\infty \leq h^{-d/2}\|\nabla_h \boldsymbol{e}_h^n\|_2$;
- Summation by parts: $\langle -\Delta_h \boldsymbol{f}_h, \boldsymbol{g}_h\rangle = \langle \nabla_h \boldsymbol{f}_h, \nabla_h \boldsymbol{g}_h\rangle$;
- Discrete Gronwall inequality: Let $\{\alpha_j\}_{j\geq 0}$, $\{\beta_j\}_{j\geq 0}$ and $\{\omega_j\}_{j\geq 0}$ be sequences of real numbers such that

$$\alpha_j \leq \alpha_{j+1}, \quad \beta_j \geq 0, \quad and \quad \omega_j \leq \alpha_j + \sum_{i=0}^{j-1} \beta_i \omega_i, \quad \forall j \geq 0.$$

  Then it holds that

$$\omega_j \leq \alpha_j \exp\left\{\sum_{i=0}^{j-1} \beta_i\right\}, \quad \forall j \geq 0.$$

Discrete gradient acting on cross product

Lemma

For grid functions $\boldsymbol{f}_h$ and $\boldsymbol{g}_h$ over the uniform numerical grid, we have

$$\|\nabla_h(\boldsymbol{f}\times\boldsymbol{g})_h\|_2^2 \le \mathcal{C}\Big(\|\boldsymbol{f}_h\|_\infty^2\cdot\|\nabla_h\boldsymbol{g}_h\|_2^2+\|\boldsymbol{g}_h\|_\infty^2\cdot\|\nabla_h\boldsymbol{f}_h\|_2^2\Big),$$

$$\langle(\boldsymbol{f}_h\times\Delta_h\boldsymbol{g}_h)\times\boldsymbol{f}_h,\boldsymbol{g}_h\rangle=\langle\boldsymbol{f}_h\times(\boldsymbol{g}_h\times\boldsymbol{f}_h),\Delta_h\boldsymbol{g}_h\rangle\,,$$

$$\langle\boldsymbol{f}_h\times(\boldsymbol{f}_h\times\boldsymbol{g}_h),\boldsymbol{g}_h\rangle=-\|\boldsymbol{f}_h\times\boldsymbol{g}_h\|_2^2.$$

Unconditional unique solvability

Theorem

Given $\boldsymbol{p}_h$, $\tilde{\boldsymbol{p}}_h$ and $\hat{\boldsymbol{m}}_h$, the numerical schemes

$$\Big(\frac{3}{2}I_h - \frac{3}{2}\alpha\hat{\boldsymbol{m}}_h \times I_h + k\hat{\boldsymbol{m}}_h \times \Delta_h\Big)\boldsymbol{m}_h = \boldsymbol{p}_h,$$

$$\Big(\frac{3}{2}I_h + k\hat{\boldsymbol{m}}_h \times \Delta_h + \alpha k\hat{\boldsymbol{m}}_h \times (\hat{\boldsymbol{m}}_h \times \Delta_h)\Big)\boldsymbol{m}_h = \tilde{\boldsymbol{p}}_h,$$

are uniquely solvable.

Denote $\boldsymbol{q}_h = -\Delta_h\boldsymbol{m}_h$. Then

$$\boldsymbol{m}_h = (-\Delta_h)^{-1}\boldsymbol{q}_h + C^*_{\boldsymbol{q}_h} \quad \text{with } C^*_{\boldsymbol{q}_h} = \frac{2}{3}\Big(\overline{\tilde{\boldsymbol{p}}_h} + k\overline{\hat{\boldsymbol{m}}_h \times \boldsymbol{q}_h} + \alpha k\overline{\hat{\boldsymbol{m}}_h \times (\hat{\boldsymbol{m}}_h \times \boldsymbol{q}_h)}\Big)$$

and

$$G(\boldsymbol{q}_h) := \frac{3}{2}((-\Delta_h)^{-1}\boldsymbol{q}_h + C^*_{\boldsymbol{q}_h}) - \tilde{\boldsymbol{p}}_h - k\hat{\boldsymbol{m}}_h \times \boldsymbol{q}_h - \alpha k\hat{\boldsymbol{m}}_h \times (\hat{\boldsymbol{m}}_h \times \boldsymbol{q}_h) = \boldsymbol{0}.$$

Proof

Observe that

$$A := \frac{3}{2}\alpha\hat{\boldsymbol{m}}_h \times I_h + k\hat{\boldsymbol{m}}_h \times (-\Delta_h)$$
$$= k\hat{\boldsymbol{m}}_h \times \left(-\Delta_h + \frac{3\alpha}{2k} I_h\right)$$
$$=: kMS.$$

- I_h: identity matrix; M: antisymmetric matrix;
- $S = -\Delta_h + \frac{3\alpha}{2k} I_h$: symmetric positive definite matrix;
- $S = C^T C$ with C being nonsingular;
- $|\lambda I - MS| = |\lambda I - MC^T C| = |\lambda I - CMC^T|$;
- $(CMC^T)^T = -CMC^T$;

Lemma (spectral lemma for antisymmetric matrices)

Each eigenvalue of the real skew-symmetric matrix is either 0 *or purely imaginary number.*

Continued ...

By the lemma, $\det(\frac{3}{2}I_h - \frac{3}{2}\alpha\hat{\boldsymbol{m}}_h \times I_h + k\hat{\boldsymbol{m}}_h \times \Delta_h) \neq 0$ since the matrix has $\frac{3}{2}$ as real parts, and thus the corresponding linear system of equations has a unique solution.
For any $\boldsymbol{q}_{1,h}$, $\boldsymbol{q}_{2,h}$ with $\overline{\boldsymbol{q}_{1,h}} = \overline{\boldsymbol{q}_{2,h}} = 0$, we denote $\tilde{\boldsymbol{q}}_h = \boldsymbol{q}_{1,h} - \boldsymbol{q}_{2,h}$

$$\begin{aligned}
&\langle G(\boldsymbol{q}_{1,h}) - G(\boldsymbol{q}_{2,h}), \boldsymbol{q}_{1,h} - \boldsymbol{q}_{2,h}\rangle \\
&= \frac{3}{2k}\Big(\langle(-\Delta_h)^{-1}\tilde{\boldsymbol{q}}_h, \tilde{\boldsymbol{q}}_h\rangle + \langle C^*_{\boldsymbol{q}_{1,h}} - C^*_{\boldsymbol{q}_{1,h}}, \tilde{\boldsymbol{q}}_h\rangle\Big) \\
&- \langle\hat{\boldsymbol{m}}_h \times \tilde{\boldsymbol{q}}_h, \tilde{\boldsymbol{q}}_h\rangle - \alpha\langle\hat{\boldsymbol{m}}_h \times (\hat{\boldsymbol{m}}_h \times \tilde{\boldsymbol{q}}_h), \tilde{\boldsymbol{q}}_h\rangle \\
&\geq \frac{3}{2k}\Big(\langle(-\Delta_h)^{-1}\tilde{\boldsymbol{q}}_h, \tilde{\boldsymbol{q}}_h\rangle + \langle C^*_{\boldsymbol{q}_{1,h}} - C^*_{\boldsymbol{q}_{2,h}}, \tilde{\boldsymbol{q}}_h\rangle\Big) \\
&= \frac{3}{2k}\langle(-\Delta_h)^{-1}\tilde{\boldsymbol{q}}_h, \tilde{\boldsymbol{q}}_h\rangle = \frac{3}{2k}\|\tilde{\boldsymbol{q}}_h\|_{-1}^2 \geq 0.
\end{aligned}$$

Continued ...

Moreover, for any $\boldsymbol{q}_{1,h}$, $\boldsymbol{q}_{2,h}$ with $\overline{\boldsymbol{q}_{1,h}} = \overline{\boldsymbol{q}_{2,h}} = 0$, we get

$$\langle G(\boldsymbol{q}_{1,h}) - G(\boldsymbol{q}_{2,h}), \boldsymbol{q}_{1,h} - \boldsymbol{q}_{2,h} \rangle \geq \frac{3}{2k} \|\tilde{\boldsymbol{q}}_h\|_{-1}^2 > 0, \quad \text{if } \boldsymbol{q}_{1,h} \neq \boldsymbol{q}_{2,h},$$

and the equality only holds when $\boldsymbol{q}_{1,h} = \boldsymbol{q}_{2,h}$.

Lemma (Browder-Minty lemma [Browder, 1963, Minty, 1963])

Let X be a real, reflexive Banach space and let $T : X \to X'$ (the dual space of X) be bounded, continuous, coercive (i.e., $\frac{(T(u),u)}{\|u\|_X} \to +\infty$, as $\|u\|_X \to +\infty$) and monotone. Then for any $g \in X'$ there exists a solution $u \in X$ of the equation $T(u) = g$. Furthermore, if the operator T is strictly monotone, then the solution u is unique.

By the Browder-Minty lemma, the semi-implicit scheme admits a unique solution.

Optimal rate convergence analysis [Chen, Wang and Xie, submitted, 2019]

Theorem

Let $\boldsymbol{m}_e \in C^3([0,T];C^0) \cap L^\infty([0,T];C^4)$ *be a smooth solution with the initial data* $\boldsymbol{m}_e(\boldsymbol{x},0) = \boldsymbol{m}_e^0(\boldsymbol{x})$ *and* $\boldsymbol{m}_h$ *be the numerical solution with the initial data* $\boldsymbol{m}_h^0 = \boldsymbol{m}_{e,h}^0$ *and* $\boldsymbol{m}_h^1 = \boldsymbol{m}_{e,h}^1$. *Suppose that the initial error satisfies* $\|\boldsymbol{m}_{e,h}^\ell - \boldsymbol{m}_h^\ell\|_2 + \|\nabla_h(\boldsymbol{m}_{e,h}^\ell - \boldsymbol{m}_h^\ell)\|_2 = \mathcal{O}(k^2+h^2)$, $\ell = 0,1$, *and* $k \le \mathcal{C}h$. *Then the following convergence result holds as* h *and* k *goes to zero:*

$$\|\boldsymbol{m}_{e,h}^n - \boldsymbol{m}_h^n\|_2 + \|\nabla_h(\boldsymbol{m}_{e,h}^n - \boldsymbol{m}_h^n)\|_2 \le \mathcal{C}(k^2+h^2), \quad \forall n \ge 2,$$

in which the constant $\mathcal{C} > 0$ *is independent of* k *and* h.

Idea of the proof

- Initial error: $\boldsymbol{e}_h^0$ and $\boldsymbol{e}_h^1$;
- Alternative estimate: Using discrete Gronwall inequality and another lemma to evaluate $\tilde{\boldsymbol{e}}_h$ and $\nabla_h \tilde{\boldsymbol{e}}_h$; Again by the lemma to estimate $\boldsymbol{e}_h$ and $\nabla_h \boldsymbol{e}_h$. Illustrated by the following schematic:

$$
\begin{tikzcd}
 & \|\tilde{\boldsymbol{e}}_h^2\|, \|\nabla_h \tilde{\boldsymbol{e}}_h^2\| \arrow[dr] & \|\tilde{\boldsymbol{e}}_h^3\|, \|\nabla_h \tilde{\boldsymbol{e}}_h^3\| \arrow[dr] & \|\tilde{\boldsymbol{e}}_h^4\|, \|\nabla_h \tilde{\boldsymbol{e}}_h^4\| & \cdots \\
\|\boldsymbol{e}_h^0\|, \|\nabla_h \boldsymbol{e}_h^0\| \arrow[r, dashed] & \|\boldsymbol{e}_h^1\|, \|\nabla_h \boldsymbol{e}_h^1\| \arrow[u] \arrow[r, dashed] & \|\boldsymbol{e}_h^2\|, \|\nabla_h \boldsymbol{e}_h^2\| \arrow[u] \arrow[r, dashed] & \|\boldsymbol{e}_h^3\|, \|\nabla_h \boldsymbol{e}_h^3\| \arrow[u] & \cdots
\end{tikzcd}
$$

- To guarantee the assumptions in the recursive demonstration.

Sketch of the proof

Step 1: Construction of an approximate solution $\underline{\boldsymbol{m}}$:

$$\underline{\boldsymbol{m}} = \boldsymbol{m}_e + h^2 \boldsymbol{m}^{(1)},$$

in which the auxiliary field $\boldsymbol{m}^{(1)}$ satisfies

$$\Delta \boldsymbol{m}^{(1)} = \hat{C} \quad \text{with } \hat{C} = \frac{1}{|\Omega|} \int_{\partial\Omega} \partial_\nu^3 \boldsymbol{m}_e \, \mathrm{d}s,$$

$$\partial_z \boldsymbol{m}^{(1)} \mid_{z=0} = -\frac{1}{24} \partial_z^3 \boldsymbol{m}_e \mid_{z=0}, \quad \partial_z \boldsymbol{m}^{(1)} \mid_{z=1} = \frac{1}{24} \partial_z^3 \boldsymbol{m}_e \mid_{z=1} .$$

Then

$$\boldsymbol{m}_e(\hat{x}_i, \hat{y}_j, \hat{z}_0) = \boldsymbol{m}_e(\hat{x}_i, \hat{y}_j, \hat{z}_1) - \frac{h^3}{24} \partial_z^3 \boldsymbol{m}_e(\hat{x}_i, \hat{y}_j, 0) + \mathcal{O}(h^5),$$

$$\boldsymbol{m}^{(1)}(\hat{x}_i, \hat{y}_j, \hat{z}_0) = \boldsymbol{m}^{(1)}(\hat{x}_i, \hat{y}_j, \hat{z}_1) + \frac{h}{24} \partial_z^3 \boldsymbol{m}_e(\hat{x}_i, \hat{y}_j, 0) + \mathcal{O}(h^3),$$

$$\underline{\boldsymbol{m}}(\hat{x}_i, \hat{y}_j, \hat{z}_0) = \underline{\boldsymbol{m}}(\hat{x}_i, \hat{y}_j, \hat{z}_1) + \mathcal{O}(h^5),$$

$$\Delta_h \underline{\boldsymbol{m}}_{i,j,k} = \Delta \boldsymbol{m}_e(\hat{x}_i, \hat{y}_j, \hat{z}_k) + \mathcal{O}(h^2), \quad \forall 1 \le i, j, k \le N.$$

Step 2: Error function evolution system for

$$\tilde{\boldsymbol{e}}_h^n = \underline{\boldsymbol{m}}_h^n - \tilde{\boldsymbol{m}}_h^n, \quad \boldsymbol{e}_h^n = \underline{\boldsymbol{m}}_h^n - \boldsymbol{m}_h^n,$$

$$\begin{aligned}
\frac{\frac{3}{2}\tilde{\boldsymbol{e}}_h^{n+2} - 2\tilde{\boldsymbol{e}}_h^{n+1} + \frac{1}{2}\tilde{\boldsymbol{e}}_h^n}{k} &= -\left(2\boldsymbol{m}_h^{n+1} - \boldsymbol{m}_h^n\right) \times \Delta_h \tilde{\boldsymbol{e}}_h^{n+2} - \left(2\boldsymbol{e}_h^{n+1} - \boldsymbol{e}_h^n\right) \times \Delta_h \underline{\boldsymbol{m}}_h^{n+2} \\
&\quad - \alpha\left(2\boldsymbol{m}_h^{n+1} - \boldsymbol{m}_h^n\right) \times \left(\left(2\boldsymbol{m}_h^{n+1} - \boldsymbol{m}_h^n\right) \times \Delta_h \tilde{\boldsymbol{e}}_h^{n+2}\right) \\
&\quad - \alpha\left(2\boldsymbol{m}_h^{n+1} - \boldsymbol{m}_h^n\right) \times \left(\left(2\boldsymbol{e}_h^{n+1} - \boldsymbol{e}_h^n\right) \times \Delta_h \underline{\boldsymbol{m}}_h^{n+2}\right) \\
&\quad - \alpha\left(2\boldsymbol{e}_h^{n+1} - \boldsymbol{e}_h^n\right) \times \left(\left(2\underline{\boldsymbol{m}}_h^{n+1} - \underline{\boldsymbol{m}}_h^n\right) \times \Delta_h \underline{\boldsymbol{m}}_h^{n+2}\right) + \tau^{n+2}
\end{aligned}$$

with $\|\tau^{n+2}\|_2 \le C(k^2 + h^2)$.

- Discrete L^2 error estimate: Inner product with $\tilde{\boldsymbol{e}}_h^{\ell+2}$

$$\begin{aligned}
&\|\tilde{\boldsymbol{e}}_h^{\ell+2}\|_2^2 - \|\tilde{\boldsymbol{e}}_h^{\ell+1}\|_2^2 + \|2\tilde{\boldsymbol{e}}_h^{\ell+2} - \tilde{\boldsymbol{e}}_h^{\ell+1}\|_2^2 - \|2\tilde{\boldsymbol{e}}_h^{\ell+1} - \tilde{\boldsymbol{e}}_h^{\ell}\|_2^2 \\
\le\, &\mathcal{C}k(\|\nabla_h \tilde{\boldsymbol{e}}_h^{\ell+2}\|_2^2 + \|\tilde{\boldsymbol{e}}_h^{\ell+2}\|_2^2 + \|\boldsymbol{e}_h^{\ell+1}\|_2^2 + \|\boldsymbol{e}_h^{\ell}\|_2^2) + \mathcal{C}k(k^4 + h^4).
\end{aligned}$$

Remark: Discrete Gronwall inequality is not applicable due to the presence of H_h^1 norms of the error function.

- Discrete inner product with $-\Delta_h \tilde{\boldsymbol{e}}_h^{\ell+2}$

$$
\begin{aligned}
&\|\nabla_h \tilde{\boldsymbol{e}}_h^{\ell+2}\|_2^2 - \|\nabla_h \tilde{\boldsymbol{e}}_h^{\ell+1}\|_2^2 + \|2\nabla_h \tilde{\boldsymbol{e}}_h^{\ell+2} - \nabla_h \tilde{\boldsymbol{e}}_h^{\ell+1}\|_2^2 - \|2\nabla_h \tilde{\boldsymbol{e}}_h^{\ell+1} - \nabla_h \tilde{\boldsymbol{e}}_h^{\ell}\|_2^2 \\
\leq & \mathcal{C}k\Big(\|\nabla_h \tilde{\boldsymbol{e}}_h^{\ell+2}\|_2^2 + \|\nabla_h \boldsymbol{e}_h^{\ell+1}\|_2^2 + \|\nabla_h \boldsymbol{e}_h^{\ell}\|_2^2 + \|\boldsymbol{e}_h^{\ell+1}\|_2^2 + \|\boldsymbol{e}_h^{\ell}\|_2^2\Big) + \mathcal{C}k(k^4 + h^4).
\end{aligned}
$$

- Combination of both

$$
\begin{aligned}
&\|\tilde{\boldsymbol{e}}_h^{\ell+2}\|_2^2 - \|\tilde{\boldsymbol{e}}_h^{\ell+1}\|_2^2 + \|2\tilde{\boldsymbol{e}}_h^{\ell+2} - \tilde{\boldsymbol{e}}_h^{\ell+1}\|_2^2 - \|2\tilde{\boldsymbol{e}}_h^{\ell+1} - \tilde{\boldsymbol{e}}_h^{\ell}\|_2^2 \\
&+ \|\nabla_h \tilde{\boldsymbol{e}}_h^{\ell+2}\|_2^2 - \|\nabla_h \tilde{\boldsymbol{e}}_h^{\ell+1}\|_2^2 + \|\nabla_h (2\tilde{\boldsymbol{e}}_h^{\ell+2} - \tilde{\boldsymbol{e}}_h^{\ell+1})\|_2^2 - \|\nabla_h (2\tilde{\boldsymbol{e}}_h^{\ell+1} - \tilde{\boldsymbol{e}}_h^{\ell})\|_2^2 \\
\leq & \mathcal{C}k\Big(\|\nabla_h \tilde{\boldsymbol{e}}_h^{\ell+2}\|_2^2 + \|\tilde{\boldsymbol{e}}_h^{\ell+2}\|_2^2 + \|\nabla_h \boldsymbol{e}_h^{\ell+1}\|_2^2 + \|\nabla_h \boldsymbol{e}_h^{\ell}\|_2^2 + \|\boldsymbol{e}_h^{\ell+1}\|_2^2 + \|\boldsymbol{e}_h^{\ell}\|_2^2\Big) \\
&+ \mathcal{C}k(k^4 + h^4).
\end{aligned}
$$

Lemma

Consider $\underline{\boldsymbol{m}}_h = \boldsymbol{m}_e + h^2 \boldsymbol{m}^{(1)}$ *with* $\boldsymbol{m}_e$ *the exact solution and* $|\boldsymbol{m}_e| = 1$ *at a point-wise level, and* $\|\boldsymbol{m}^{(1)}\|_\infty + \|\nabla_h \boldsymbol{m}^{(1)}\|_\infty \le \mathcal{C}$. *For any numerical solution* $\tilde{\boldsymbol{m}}_h$, *we define* $\boldsymbol{m}_h = \frac{\tilde{\boldsymbol{m}}_h}{|\tilde{\boldsymbol{m}}_h|}$. *Suppose both numerical profiles satisfy the following* $W_h^{1,\infty}$ *bounds*

$$|\tilde{\boldsymbol{m}}_h| \ge \frac{1}{2}, \quad \text{at a point-wise level,}$$
$$\|\boldsymbol{m}_h\|_\infty + \|\nabla_h \boldsymbol{m}_h\|_\infty \le M, \quad \|\tilde{\boldsymbol{m}}_h\|_\infty + \|\nabla_h \tilde{\boldsymbol{m}}_h\|_\infty \le M,$$

and we denote the numerical error functions as $\boldsymbol{e}_h = \underline{\boldsymbol{m}}_h - \boldsymbol{m}_h$, $\tilde{\boldsymbol{e}}_h = \underline{\boldsymbol{m}}_h - \tilde{\boldsymbol{m}}_h$. *Then the following estimate is valid*

$$\|\boldsymbol{e}_h\|_2 \le 2\|\tilde{\boldsymbol{e}}_h\|_2 + \mathcal{O}(h^2), \quad \|\nabla_h \boldsymbol{e}_h\|_2 \le \mathcal{C}(\|\nabla_h \tilde{\boldsymbol{e}}_h\|_2 + \|\tilde{\boldsymbol{e}}_h\|_2) + \mathcal{O}(h^2).$$

- Using the Lemma

$$
\begin{aligned}
&\|\tilde{\boldsymbol{e}}_h^{\ell+2}\|_2^2 - \|\tilde{\boldsymbol{e}}_h^{\ell+1}\|_2^2 + \|2\tilde{\boldsymbol{e}}_h^{\ell+2} - \tilde{\boldsymbol{e}}_h^{\ell+1}\|_2^2 - \|2\tilde{\boldsymbol{e}}_h^{\ell+1} - \tilde{\boldsymbol{e}}_h^{\ell}\|_2^2 \\
&+ \|\nabla_h \tilde{\boldsymbol{e}}_h^{\ell+2}\|_2^2 - \|\nabla_h \tilde{\boldsymbol{e}}_h^{\ell+1}\|_2^2 + \|\nabla_h(2\tilde{\boldsymbol{e}}_h^{\ell+2} - \tilde{\boldsymbol{e}}_h^{\ell+1})\|_2^2 - \|\nabla_h(2\tilde{\boldsymbol{e}}_h^{\ell+1} - \tilde{\boldsymbol{e}}_h^{\ell})\|_2^2 \\
\le\, &\mathcal{C}k\Big(\|\nabla_h \tilde{\boldsymbol{e}}_h^{\ell+2}\|_2^2 + \|\nabla_h \tilde{\boldsymbol{e}}_h^{\ell+1}\|_2^2 + \|\nabla_h \tilde{\boldsymbol{e}}_h^{\ell}\|_2^2 + \|\tilde{\boldsymbol{e}}_h^{\ell+2}\|_2^2 + \|\tilde{\boldsymbol{e}}_h^{\ell+1}\|_2^2 + \|\tilde{\boldsymbol{e}}_h^{\ell}\|_2^2\Big) \\
&+ \mathcal{C}k(k^4 + h^4).
\end{aligned}
$$

- Discrete Gronwall inequality

$$
\|\tilde{\boldsymbol{e}}_h^{n}\|_2^2 + \|\nabla_h \tilde{\boldsymbol{e}}_h^{n}\|_2^2 \le \mathcal{C}Te^{\mathcal{C}T}(k^4 + h^4), \quad \text{for all } n : n \le \left\lfloor \frac{T}{k} \right\rfloor,
$$

$$
\|\tilde{\boldsymbol{e}}_h^{n}\|_2 + \|\nabla_h \tilde{\boldsymbol{e}}_h^{n}\|_2 \le \mathcal{C}(k^2 + h^2).
$$

Lemma

Assume the numerical error function:

$$\|\boldsymbol{e}_h^k\|_\infty + \|\nabla_h \boldsymbol{e}_h^k\|_\infty \le \frac{1}{3}, \ \ \|\tilde{\boldsymbol{e}}_h^k\|_\infty + \|\nabla_h \tilde{\boldsymbol{e}}_h^k\|_\infty \le \frac{1}{3}, \quad \textit{for } k = \ell, \ell+1.$$

Such an assumption will be recovered by the convergence analysis at time step $t^{\ell+2}$. *Then numerical solutions* $\boldsymbol{m}_h$ *and* $\tilde{\boldsymbol{m}}_h$*:*

$$\|\boldsymbol{m}_h^k\|_\infty = \|\underline{\boldsymbol{m}}_h^k - \boldsymbol{e}_h^k\|_\infty \le \|\underline{\boldsymbol{m}}_h^k\|_\infty + \|\boldsymbol{e}_h^k\|_\infty \le \mathcal{C} + \frac{1}{3},$$

$$\|\nabla_h \boldsymbol{m}_h^k\|_\infty = \|\nabla_h \underline{\boldsymbol{m}}_h^k - \nabla_h \boldsymbol{e}_h^k\|_\infty \le \|\nabla_h \underline{\boldsymbol{m}}_h^k\|_\infty + \|\nabla_h \boldsymbol{e}_h^k\|_\infty \le \mathcal{C} + \frac{1}{3},$$

$$\|\tilde{\boldsymbol{m}}_h^k\|_\infty \le \mathcal{C} + \frac{1}{3}, \quad \|\nabla_h \tilde{\boldsymbol{m}}_h^k\|_\infty \le \mathcal{C} + \frac{1}{3} \quad \textit{(similar derivation)}.$$

- Inverse inequality with time step constraint $k \le \mathcal{C}h$

$$\|\tilde{\boldsymbol{e}}_h^n\|_\infty \le \frac{\|\tilde{\boldsymbol{e}}_h^n\|_2}{h^{d/2}} \le \frac{\mathcal{C}(k^2+h^2)}{h^{d/2}} \le \frac{1}{6},$$

$$\|\nabla_h \tilde{\boldsymbol{e}}_h^n\|_\infty \le \frac{\|\nabla_h \tilde{\boldsymbol{e}}_h^n\|_2}{h^{d/2}} \le \frac{\mathcal{C}(k^2+h^2)}{h^{d/2}} \le \frac{1}{6}.$$

- Convergence estimate for $\boldsymbol{e}_h^n$:

$$\|\boldsymbol{e}_h^n\|_2 \le 2\|\tilde{\boldsymbol{e}}_h^n\|_2 + \mathcal{O}(h^2) \le \mathcal{C}(k^2+h^2),$$
$$\|\nabla_h \boldsymbol{e}_h^n\|_2 \le \mathcal{C}(\|\nabla_h \tilde{\boldsymbol{e}}_h^n\|_2 + \|\tilde{\boldsymbol{e}}_h^n\|_2) + \mathcal{O}(h^2) \le \mathcal{C}(k^2+h^2).$$

Verification of assumptions.

$$|\tilde{\boldsymbol{m}}_h| \ge \frac{1}{2}, \quad \text{at a point-wise level,}$$
$$\|\boldsymbol{m}_h\|_\infty + \|\nabla_h \boldsymbol{m}_h\|_\infty \le M, \quad \|\tilde{\boldsymbol{m}}_h\|_\infty + \|\nabla_h \tilde{\boldsymbol{m}}_h\|_\infty \le M,$$
$$\|\boldsymbol{e}_h^n\|_\infty \le \frac{1}{6}, \quad \|\nabla_h \boldsymbol{e}_h^n\|_\infty \le \frac{1}{6},$$
$$\|\tilde{\boldsymbol{e}}_h^n\|_\infty \le \frac{1}{6}, \quad \|\nabla_h \tilde{\boldsymbol{e}}p_h^n\|_\infty \le \frac{1}{6}.$$

□

Outline

Numerical examples

Homogenous Neumann boundary condition

1. 1-D example with a forcing term and the given exact solution
2. 1-D example without the exact solution
3. 3-D example with a forcing term and the given exact solution

Example 1

$$\boldsymbol{m}_e = \left(\cos(x^2(1-x)^2)\sin t, \sin(x^2(1-x)^2)\sin t, \cos t\right)^T$$

Table 2: Accuracy of our method on the uniform mesh when $h = k$ and $\alpha = 0.01$.

k	$\|\boldsymbol{m}_h - \boldsymbol{m}_e\|_\infty$	$\|\boldsymbol{m}_h - \boldsymbol{m}_e\|_2$	$\|\boldsymbol{m}_h - \boldsymbol{m}_e\|_{H^1}$
5.0D-3	3.867D-5	4.115D-5	1.729D-4
2.5D-3	7.976D-6	1.053D-5	4.629D-5
1.25D-3	2.135D-6	2.648D-6	1.177D-5
6.25D-4	5.765D-7	6.627D-7	2.949D-6
3.125D-4	1.447D-7	1.657D-7	7.370D-7
order	1.991	1.990	1.972

Example 2

Table 3: Temporal accuracy of our method on the uniform mesh when $h = 1D-4$ and $\alpha = 0.01$.

k	$\|\boldsymbol{m}_h - \boldsymbol{m}_e\|_\infty$	$\|\boldsymbol{m}_h - \boldsymbol{m}_e\|_2$	$\|\boldsymbol{m}_h - \boldsymbol{m}_e\|_{H^1}$
5.0D-3	2.949D-5	3.250D-5	1.633D-4
2.5D-3	8.116D-6	8.429D-6	4.393D-5
1.25D-3	2.125D-6	2.114D-6	1.118D-5
6.25D-4	4.851D-7	5.190D-7	2.791D-6
3.125D-4	1.129D-7	1.196D-7	6.875D-7
order	2.012	2.019	1.976

Table 4: Spatial accuracy of our method on the uniform mesh when $k = 1D-4$ and $\alpha = 0.01$.

h	$\|\boldsymbol{m}_h - \boldsymbol{m}_e\|_\infty$	$\|\boldsymbol{m}_h - \boldsymbol{m}_e\|_2$	$\|\boldsymbol{m}_h - \boldsymbol{m}_e\|_{H^1}$
$1/3^2$	0.00546	0.00577	0.01336
$1/3^3$	6.101D-4	6.430D-4	0.00160
$1/3^4$	6.782D-5	7.146D-5	1.820D-4
$1/3^5$	7.527D-6	7.930D-6	2.036D-5
$1/3^6$	8.271D-7	8.714D-7	2.243D-6
order	2.001	2.002	1.980

Example 3

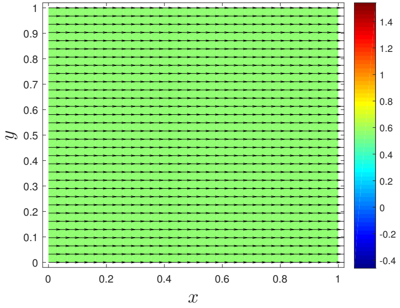

(e) Exact magnetization profile

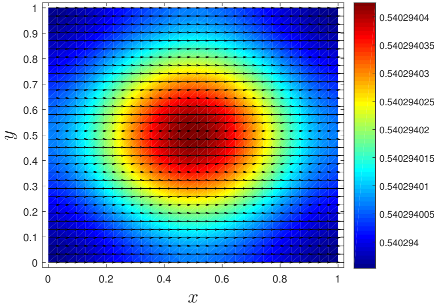

(f) Numerical magnetization profile

Figure 8: Profiles of the exact and the numerical magnetization in the $xy-$plane with $z = 1/2$ when $k = 1/256$, $h_x = h_y = h_z = 1/32$, and $\alpha = 0.01$.

Table 5: Temporal accuracy in the 3-D case when $h_x = h_y = h_z = 1/32$ and $\alpha = 0.01$.

k	$\|\boldsymbol{m}_h - \boldsymbol{m}_e\|_\infty$	$\|\boldsymbol{m}_h - \boldsymbol{m}_e\|_2$	$\|\boldsymbol{m}_h - \boldsymbol{m}_e\|_{H^1}$
1/16	1.685D-3	1.098D-3	1.211D-3
1/32	4.411D-4	2.964D-4	3.082D-4
1/64	1.128D-4	7.730D-5	7.772D-5
1/128	2.966D-5	2.024D-5	2.051D-5
1/256	8.311D-6	5.693D-6	5.812D-6
order	1.922	1.906	1.932

Outline

Conclusion

What we have done

1. Two second-order semi-implicit schemes for LL equation;
2. Benchmark problem from NIST;
3. Unique solvability for two schemes;
4. Convergence analysis for one of the schemes.

To-do list

1. Generalization of the technique for other implicit scheme;
2. Current-driven magnetization dynamics [Chen, García-Cervera, and Yang, 2015];
3. Application to Landau-Lifshitz-Maxwell equations.

Thank you